Published in final edited form as:
Biomaterials. 2011 October ; 32(29): 7159–7168. doi:10.1016/j.biomaterials.2011.06.013.

Microenvironment Induced Spheroid to Sheeting Transition of Immortalized Human Keratinocytes (HaCaT) Cultured in Microbubbles Formed in Polydimethylsiloxane

Siddarth Chandrasekaran[1], **Ut-Binh Giang**[1], **Michael R. King**[2], and **Lisa A DeLouise**[1,3,*]

[1]Department of Biomedical Engineering, University of Rochester, Goergen Hall, NY 14627, USA

[2]Department of Biomedical Engineering, Cornell University, Weill Hall, NY 14853, USA

[3]Department of Dermatology, University of Rochester Medical Center, Rochester, NY 14642, USA

Abstract

The in vivo cellular microenvironment is regulated by a complex interplay of soluble factors and signaling molecules secreted by cells and it plays a critical role in the growth and development of normal and diseased tissues. In vitro systems that can recapitulate the microenvironment at the cellular level are needed to investigate the influence of autocrine signaling and extracellular matrix effects on tissue homeostasis, regeneration, and disease development and progression. In this study we report the use of microbubble technology as a means to culture cells in a controlled microenvironment in which cells can influence their function through autocrine signaling. Microbubbles (MB) are small spherical cavities about 100–300 μm in diameter formed in hydrophobic polymer polydimethylsiloxane (PDMS) with ~60–100 μm circular openings and aspect ratio ~3.5. We demonstrate that the unique architecture of the microbubble compartment is advantaged for cell culture using HaCaT cells, an immortalized keratinocyte cell line. We observe that HaCaT cells, seeded in microbubbles (15–20 cells / MB) and cultured under standard conditions, adopt a compact 3-D spheroidal morphology. Within 2–3 days, the cells transition to a sheeting morphology. Through experimentation and simulation we show that this transition in morphology is due to the unique architecture of the microbubble compartment which enables cells to condition their local microenvironment. The small media volume per cell and the development of shallow concentration gradients allow factors secreted by the cells to rise to bioactive levels. The kinetics of the morphology transition depends on the number of cells seeded per microbubble; higher cell seeding induces a more rapid transition. HaCaT cells seeded onto PDMS cured in 96-well plates also form compact spheroids but they do not transition to a sheeting morphology even after several weeks of culture. The importance of soluble factor accumulation in driving this morphology transition in microbubbles is supported by the observation that spheroids do not form when cells - seeded into microbubbles or onto PDMS cured in 96 well plates - are cultured in media conditioned by HaCaT cells grown in standard tissue culture plate. We observed that the addition of TGF-β1 to the growth media induced cells to proliferate in a sheeting morphology from the onset both on PDMS cured in 96-well plates and in microbubbles. TGF-β1 is a

*Correspondence should be addressed to, Lisa A. DeLouise (lisa_delouise@urmc.rochester.edu), University of Rochester Medical Center, Department of Dermatology Box 697, 601 Elmwood Ave, Lab 6-6823, Rochester, NY 14642, Phone: 585-275-1810, Fax: 585- 273-1346.

morphogen known to regulate epithelial-to-mesenchymal transition (EMT). Studies of the role of Ca^{2+} concentration and changes in Ecadherin expression additionally support an EMT-like HaCaT morphology transition. These findings taken together validate the microbubble compartment as a unique cell culture platform that can potentially transform investigative studies in cell biology and in particular the tumor microenvironment. Targeting the tumor microenvironment is an emerging area of anti-cancer therapy.

Keywords

Cell spreading; Polydimethylsiloxane; Cell culture; Transforming Growth Factor (TGF)

1. Introduction

One of the primary determining factors of the activity of a cell in the human body is the cellular microenvironment, which is a complex network of proteins and signaling molecules that are crucial in the regulation of intercellular communications amongst different cell types. Microenvironmental cues impact the ability of cells to adapt to the local environment. They influence cell morphology [1–3] and have been inextricably linked to several physiological functions such as normal organ development [4] and stem cell maintenance [5]. Microenvironmental cues also drive pathologic conditions. In cancer, the tumor microenvironment is characterized by intercellular interactions (i.e. cell-cell and cell-extracellular matrix (ECM) contacts), the chemical environment (i.e., soluble factors secreted by the cells and the dynamics of nutrient and waste flux) and the mechanical aspects of the local geometry [6, 7]. The tumor microenvironment has been shown to dramatically influence the course of tumor progression [8], metastasis [9–11] and generation of tumor initiating cells [12]. Thus, clarifying all the aspects of cell microenvironment is essential for understanding tissue regeneration and developing new therapeutic approaches for fighting disease [12, 13].

Studying the cellular microenvironment and its role in vitro has been challenging due to a lack of tools that can independently manipulate the components and properties of the microenvironment at the cellular level. The use of standard tissue culture to understand the role of the cellular microenvironment in cancer, angiogenesis and other important physiological processes has been limited by the loss of cellular in vivo responses and functions in the in vitro setting [14]. Over the past decade application of microfabrication to develop cell culture platforms employing biocompatible polymers has been seen as an approach to overcome these limitations [15–17]. Many methods involve the usage of printed arrays composed of ECM proteins and other morphogens [18, 19]. The major issue with these technologies is that they take into account only the insoluble component of the microenvironment and do not include the soluble factors that are secreted by the cells. This can be overcome by the use of micro-bioreactor arrays perfused with controlled culture media [20] but these systems require the use of highly complicated and expensive experimental setups for maintaining the flow parameters. Thus, there is an unmet need for a simple yet inexpensive platform that allows for control of the insoluble extracellular matrix and enables cells to condition the microenvironment through secretion of soluble factors.

In this study we show that microbubble arrays fabricated in polydimethylsiloxane (PDMS) can be used as a cell culture platform with a controlled microenvironment in which seeded cells secrete soluble factors to influence their function. PDMS is a common silicone based elastomer whose properties include chemical inertness, biocompatibility, high gas permeability, transparency, and high fidelity molding. Due to these characteristics, PDMS has been used in a variety of microfluidic devices for biological studies [21, 22] and for cell

culture [23]. PDMS microbubble technology uniquely incorporates the established benefits of microfabrication including cost-effective scalability (microbubble size and density per chip), arrayed format, and microfluidic integration combined with the advantages of customizable surface chemistry, and a high radius of curvature which we exploit for cell culture studies. As previously described [24, 25], spherical microbubble compartments (typically 100–300 μm in diameter) are formed by the gas expansion molding (GEM) technique that requires a deep reactive ion etched (DRIE) silicon wafer mold, a hydrophobic coating, and a rapid thermal cure. Previous results suggested that the formation of these bubbular compartments is a uniform and controlled process [25].

In this work we explore potential advantages of the unique microbubble geometry to enable studies of how cells interact with and condition their 3D microenvironment. Microbubbles are formed in PDMS which is a low surface energy substrate that is not conducive to cell adhesion. Hydrophobic surfaces are often used to generate multicellular spheroids [26, 27] for studying cancer processes such as the epithelial-mesenchymal-transition (EMT); a process whereby a polarized epithelial cell transitions to migratory mesenchymal phenotype. EMT is a critical step, highly regulated by the tumor microenvironment that imparts migratory potential to cancer cells necessary for metastasis [28–32]. We hypothesize that the microbubble well is uniquely suited to study the EMT process due to the low media volume per cell ratio which will allow cells to condition their microenvironment through autocrine signaling. This work will demonstrate microbubble technology to be a useful in vitro tool to study 3D interactions and the tissue microenvironment to elucidate important physical and soluble factors that regulate normal and diseased tissue development.

2. Materials and Methods

2.1 PDMS microbubble fabrication and casting PDMS in 96 well plates

To develop microbubble arrays in PDMS as a versatile cell culture platform we designed a silicon wafer mold layout using AutoCAD LT 2008 (Autodesk Inc., USA) that had 100 μm diameter circular shaped openings spaced 400 μm apart in 10×10 arrays. The silicon wafer was etched to 150 μm depth using the Bosch deep reactive ion etch (DRIE) process (Plasma Therm 770, MEMS and Nanotechnology Exchange LLC, Reston, Virginia). The DRIE silicon wafer was received after the Bosch process with the resist layer intact. This wafer was used directly to mold PDMS microbubble arrays with *Dow Corning*'s Sylgard® 184 silicone elastomer kit in a 10:1 base to curing agent ratio (w/w). The pre-polymer components were manually mixed with a pipette tip in a 50 mL tube for 30 seconds and poured onto the silicon wafer mold. The mixture was allowed to self-level for 30 minutes at room temperature, and then rapidly cured at 100 °C for 2 hours. The cured polymer with formed microbubbles is then peeled carefully and cut into small chips (1 cm × 0.5 cm) and used in cell culture experiments. Typical chip thickness is 1 mm and each chip contained 200 microbubble wells.

For studies performed in PDMS-cured 96-well plates, 50 μL of the PDMS pre-polymer was pipetted into each well and allowed to settle at room temperature for 30 min. The plates were then cured at 40 °C for 4 hours. This lower curing temperature was used to ensure that the tissue culture plate remained unchanged by the curing process. PDMS cured in 96-well plate will be termed planar PDMS in the rest of this paper.

2.2 Cell line and cell culture

All experiments were conducted with HaCaT cells, an immortalized human keratinocyte cell line, cultured at 37°C with 5% CO_2 in Dulbecco's Modified Eagle Medium (DMEM) (Gibco 11995-060, Invitrogen Corp., USA) supplemented with 5% heat inactivated Fetal Bovine

Serum (Gibco 10082-147, Invitrogen Corp., USA) and 1% Penicillin/Streptomycin (PS) (Gibco 15140-122, Invitrogen Corp., USA). All microbubble cell seeding protocols described below were conducted in a hepafiltered tissue culture hood (SterilGARD III Advance, The Baker Company).

For cell culture experiments using PDMS microbubble arrays, small chips containing microbubbles, were rinsed with ethanol and distilled water and blown dry with nitrogen. Microbubble chips were placed in standard 24 well tissue culture plates (TCP) for cell culture experiments. To keep the chips adhered to the plate and submerged in the media during cell culture, the bottom side of the chips (opposite to the side with the microbubbles) was rendered hydrophilic by treating with atmospheric air plasma (March Plasmod GCM 200) for 10 min at 20 W. Once a chip was placed in the 24 well TCP, the top side of the chip was blocked with 50 μL of 1% bovine serum albumin (BSA, Hyclone SH30574.01, Thermo Scientific, USA) for 10 min. To replace the air trapped inside the microbubbles with cell culture media, we utilized the Vacuum-Assisted Coating (VAC) technique previously described [25]. Briefly, 40 μL of sterile 1x PBS was pipetted onto the BSA blocked chips and the TCP with microbubble chips was placed in a desktop vacuum chamber for 30 min. Application of negative pressure (−690 mm Hg relative to atmospheric pressure) depletes the air trapped in the microbubbles allowing PBS to enter the microbubbles. A reagent exchange process was used to replace the PBS with cell culture media by removing most of the PBS with a pipette - being careful not to deprime the microbubbles - and replacing it with 50 μL of cell culture media. For seeding cells into the microbubble, HaCaT cells grown to confluence in T-25 TCP were trypsinized and centrifuged at 1000xg for 10 min and re-suspended in 2 mL of cell culture media. This cell solution (50 μL) was applied to the chip (A=0.5 cm^2) for 15 min at a seeding density of 2×10^4 cells / cm^2, unless specified otherwise. This protocol seeds about 20 cells per microbubble. After seeding, the cell solution was removed and the chip was rinsed twice by placing and removing 50 μL of media on the chip. This step was done to remove cells that may have deposited onto the planar surface of the microbubble chip. The chips were carefully transferred with forceps into a different well in a 24-well TCP filled with 1 mL of media. The 24-well plate containing the microbubble chips seeded with cells was then incubated at 37°C and 5% CO_2. Culture media was changed every four days. For cell culture on planar PDMS, 100 μL of cell solution was pipetted into each well in a 96-well plate (A=0.32 cm^2) cured with PDMS at a seeding density of 2×10^4 cells / cm^2.

2.3 Varying the number of cells per microbubble

To determine the effect of the number of cells per microbubble on the kinetics of HaCaT morphology transition we varied the cell seeding concentration and the incubation time independently in the above mentioned microbubble cell seeding protocol. In one approach, the incubation time was kept constant at 15 min, while the concentration of cells in the stock solution was varied. We studied four different seeding densities (0.5, 1, 2 and 4×10^4 cells / cm^2). In a second approach, the seeding concentration was kept constant at 2×10^4 cells / cm^2 while the incubation time was varied (2, 5, 10 and 15 min).

2.4 Cell viability staining, fluorescence and multiphoton microscopy

To assess the viability of HaCaT cells cultured in microbubbles and on planar PDMS, staining experiments were performed using calcein-AM and propidium iodide (PI) at 1.0 μM and 1.5 μM, respectively. For cells cultured in microbubbles, chips submerged in culture media were taken out from the 24-well plate, excess media was removed and incubated in the dark with 50 μL of 1× PBS containing calcein-AM and PI for 30 min. After incubation, the chips were washed twice with 1× PBS to remove any excess dye that might hinder fluorescent observation. Chips were immediately imaged or stored in 1% BSA in

1xPBS. For cells cultured on planar PDMS, media was carefully removed from the 96-well plate to minimize loss of non-adherent cells. Then 100 μL of fresh media containing calcein-AM and PI was added, the plate was incubated in the dark for 30 min, and imaged using a fluorescent microscope. Wash steps were not utilized to limit loss of non-adherent cells. Fluorescent images were taken using a fluorescent microscope (Olympus IX70 with Q-Imaging Regita EXi camera and mercury lamp excitation).

In addition to 2D fluorescent images, multiphoton microscopy was used to produce 3D renderings of the cells growing in microbubbles. This was particularly useful to observe the morphological changes that the cells underwent when grown in microbubbles. Multiphoton microscopy has the capability to collect images hundreds of micrometers into biological samples and is ideally suited for imaging cells in microbubbles. Multiphoton images were captured using a multiphoton microscope (Olympus Fluo-view FV 1000 AOM-MPM) with band pass filters 519/26nm (OPI#08) for calcein-AM and 565/40nm (OPI#11) for propidium iodide.

2.5 COMSOL simulation study

Two dimensional mass transport simulations were conducted using the chemical engineering module of COMSOL Multiphysics (COMSOL, USA) to investigate the effect of the well aspect ratio on the diffusion of soluble factors secreted by a cell cultured in microbubbles and rectilinear wells. We simulated the diffusion of a soluble factor secreted by a hypothetical 10 μm cell (source) placed at the bottom of a well. Specifically, we investigated differences in the concentration profiles between microbubbles and rectilinear wells as a function of well geometry. In all cases, microbubble and rectilinear wells simulated had a constant opening diameter of 100 μm. The rectilinear well depth and the microbubble diameter were varied between 50 to 2000 μm. This corresponds to varying the aspect ratio (depth to opening diameter) from 0.5 to 20. The initial boundary conditions were set at the cell source (c = 1 nM) and all the walls (c = 0 nM). As a model secreted factor, we simulated epidermal growth factor (EGF) whose free diffusion coefficient in media ($D = 16.6 \times 10^{-7}$ cm^2 / s) was determined by others [33]. The diffusion equation was solved to determine the concentration as a function of time until steady state was reached.

2.6 Effects of conditioned media, TGF-β1 and calcium on HaCaT morphology

To investigate the effect of soluble factor accumulation we studied the morphology of HaCaT cells cultured under different media conditions in both microbubbles and on planar PDMS. We compared the morphology of HaCaTs cultured in (1) normal media (DMEM with 5% FBS and 1% PS, referred to as DMEM for simplicity), (2) media conditioned by HaCaT cells cultured in TCP termed as conditioned DMEM, (3) DMEM with 10 ng/mL of TGF-β1 and (4) calcium-free DMEM (Gibco 21068, Invitrogen Corp., USA).

Conditioned media was obtained from HaCaT cells cultured in a T-25 flask. When cells were 70–80% confluent, media was exchanged and after an overnight incubation the conditioned media was collected and used in a dilution series with normal DMEM. Cells were seeded onto planar PDMS varying the ratio of conditioned DMEM to DMEM ranging from 0 to 100%. The effect of conditioned media (100%) was also tested on cells cultured in microbubbles.

As described previously, many studies indicate that HaCaT cells actively secrete TGF-β1 into the culture media and TGF-β1 is known to repress E-Cadherin expression in keratinocytes and increase their migratory potential [32]. This suggests that TGF-β1 may be a factor contributing to the HaCaT morphology transition in microbubbles. To test this we

added 10 ng/mL [34] of human TGF- β1 (100-B-001, R&D Systems Inc.) to DMEM and observed the effect on the morphology of HaCaTs on planar PDMS and in microbubbles.

Another factor that we investigated was the influence of the calcium level in the culture media. Calcium is an important secondary messenger in many signaling pathways [35] and is required to form cell-cell adhesions through E-cadherin binding [36]. Hence, we investigated the morphology of HaCaTs on planar PDMS and microbubbles when cultured in calcium-free DMEM.

2.7 E-cadherin expression study

To test whether the change in morphology of HaCaT cells cultured in microbubbles is related to EMT, we investigated the expression of E-cadherin. Briefly, microbubble chips placed in 24 well TCP were transferred into wells containing 1× PBS. They were incubated in wells containing fixative containing Triton ×100 for 20 minutes. The chips were then transferred to 60 mm tissue culture plates and blocked with 1% BSA (Hyclone SH30574.01, Thermo Scientific, USA) for 30 minutes to prevent any nonspecific adsorption of the antibodies against E-Cadherin. After removing the BSA solution, 100μL of 1:500 dilution of FITC conjugated E-Cadherin (Anti-human CD324, Biolegend 324103) in a staining buffer composed of 1% BSA, 0.1% Sodium Azide in 1× PBS was pipetted onto the top of the chip. The tissue culture plate was incubated for 60 minutes in the dark. Then, the excess antibody solution was removed and the chip rinsed twice with 1× PBS. The chip was stored in 1% BSA and imaged using a fluorescent microscope (Olympus IX70 with Q-Imaging Regita EXi camera and mercury lamp excitation).

2.8 Statistical Analysis

All data and images reported are the results from a minimum of 3 experimental trials. Unpaired Student's t tests were performed to evaluate for statistical significance.

3. Results

3.1 Morphology of HaCaT cells on TCP, planar PDMS and in microbubbles

HaCaT cells were seeded at a density of 2×10^4 cells / cm^2 on TCP, planar PDMS, and in microbubbles as described in Section 2.2. Results indicated that HaCaT cells propagate as a monolayer on TCP (Fig. 1A), however, on planar hydrophobic PDMS, they migrate to form a single compact spheroid by the end of 24 hours (Fig. 1B). Plasma treated TCP is hydrophilic which favors cell adhesion and spreading whereas PDMS is a hydrophobic elastomer [37] that hinders HaCaT adhesion, causing cells to adopt a 3D spheroid morphology. Cell viability staining of HaCaT cells cultured on planar hydrophobic PDMS indicated a live cell periphery and dead cell core for a spheroid size ~300 μm diameter (Fig. 1C) as expected [38]. Interestingly, HaCaT cells seeded in microbubbles (Fig. 1D) also formed spheroids by the end of 24 hours (Fig. 1E). If PDMS microbubbles were pretreated with atmospheric plasma, then HaCaT cells tend to adopt a sheeting morphology from the onset (Supplementary Fig. 1S). We observed that seeding 10–15 cells per 250 μm diameter microbubble (~8 nL) formed a spheroid ~60μm in diameter after 24 hours. Interestingly, by the end of ~72 hours a fascinating transition to a sheeting morphology occurred (Fig. 1F). Within a few days HaCaT cells formed an epithelial sheet covering the internal surface area of the microbubble. Multiphoton microscope images (Fig.2) and movies (Supplementary M1 and M2) of the distinct morphologies are shown on two different microbubbles from top (I) and side (II) at the end of 24 hours (Figs. 2A, C) and 96 hours (Figs. 2B, D). By the end of 96 hours HaCaT cells uniformly sheet along the surface of microbubble. Cells were stained with live/dead markers, Calcein-AM and PI, and results indicate that, unlike spheroids on planar PDMS which were about 250 μm in diameter, all the cells were alive in a 60 μm

HaCaT spheroid in the microbubble. It is interesting to note that the spheroid to sheeting morphology transition did not occur when cells were cultured on planar PDMS even with prolonged culture up to 6 days after which spheroids appear necrotic (Supplementary Fig. 2S). To rule out any possible conditioning of the PDMS substrate by the media (serum protein deposition etc.) that could lead to sheeting of cells, we incubated planar PDMS and microbubbles with cell culture media for 72h and then seeded HaCaT cells. Results indicated that media incubation did not alter spheroid formation (Supplementary Fig. 3S). Hence, we attribute the ability of HaCaT cells to undergo morphology change in microbubbles and not on planar PDMS in a 96 well to the accumulation of soluble factors secreted by the cells that rise to bioactive levels effecting cell function. In the rest of this paper, we discuss the factors that regulate this change in morphology.

3.2 Effect of cell number per microbubble on kinetics of HaCaT morphology transition

To investigate the HaCaT spheroid to sheeting transition, we tested the effect of the number of cells seeded in the microbubble. We hypothesized that increasing the number of cells per microbubble would decrease the time to accumulate soluble factor at bioactive levels thereby impacting the kinetics of the morphology transition. As described in Section 2.3, we used two different approaches to vary the number of cells per microbubble. A summary of seeding results for the two different approaches are given in Figs. 3A, B. As expected, the number of cells per microbubble increases with increasing seeding density for a fixed incubation time ranging on average between 5 and 25 cells (Fig. 3A). The number of cells per microbubble also increases with increasing incubation time for a fixed seeding density ranging on average between 2 to 15 cells (Fig. 3B). To investigate the kinetics of the morphology transition, we seeded microbubble arrays with varying number of cells by both methods and monitored the percentage of microbubbles (n=114) showing spheroid or sheeting morphology at different time points (Figs. 3C, D). Interestingly, results indicated foremost that there is a lower limit to the number of cells per microbubble (~8 nL) required for cell survival and spheroid formation. For low seeding densities (0.5 and 1×10^4 cells / cm^2 or an average of 5 and 8 cells per microbubble, respectively) and/or shorter incubation times (2 and 5 min or an average of 2 and 5 cells per microbubble, respectively), cells did not form spheroids. By the end of 24 hours it appeared that most cells failed to thrive and eventually died. Robust cell survival and proliferation repeatedly occurred with 10 or more cells seeded per microbubble (~8 nL). This suggests that for cell survival in a hydrophobic microbubble the media volume/cell ratio must be approximately 1 nL/cell or less. However, if the microbubble was rendered hydrophilic by plasma oxidation a single cell was able to survive and proliferate inside this microbubble adopting a sheeting morphology (Supplementary Fig. 4S). Kinetic studies suggest that spheroid formation and the subsequent transition to sheeting morphology is a phenomenon that only occurs in hydrophobic microbubbles at higher seeding densities (10–25 cells per microbubble) and that the initial formation of spheroids and the time required to transition to a sheeting morphology depends on cell seeding density. Complete transition to sheeting morphology occurred within 48 hours after seeding ~25 cells per microbubble, whereas at intermediate seeding densities (~13 cells per microbubble) the transition was only ~20% complete within 48 hours (Fig. 3). These observations suggest that the ability of secreted soluble factor to rise to bioactive levels critically depends on the media volume to cell ratio.

3.3 Simulations of cell secreted soluble factor accumulation in microbubble

To gain further insight into the unique microbubble architecture for cell culture we conducted 2D mass transport simulations using COMSOL Multiphysics to quantify the diffusion of a soluble factor secreted by a hypothetical 10 μm cell (source) placed at the bottom of both rectilinear and microbubble wells with varying aspect ratios. These simulations provide insight into the physical mechanism that confers microbubbles with a

significant functional advantage of over rectilinear wells of similar size. At equilibrium, the concentration profiles at the well openings, vertically through the wells, and the integrated concentration in the wells were examined. Results showed a general trend that the vertical concentration profiles are steep for rectilinear wells and shallow for microbubbles (Fig. 4A). For wells with aspect ratio <1 both rectilinear and microbubble structures readily leak soluble factor out of the well (Figs. 4 B,C). For wells with aspect ratio >1 the concentration gradient in rectilinear wells is steep which results in depletion of secreted factor at the well opening (Fig. 4D). In contrast, the architecture of the microbubble and its increased volume produces a shallower concentration gradient that allows for accumulation of soluble factor within and at the microbubble opening (Fig. 4E). The aspect ratio of microbubbles used in our experimental studies is ~3 for which we estimate a ~4X higher concentration of soluble factor within the microbubble compared to a rectilinear well of an equivalent aspect ratio (Supplementary Fig. 5S). In summary, these simulations suggest that the microbubble architecture is less prone to suffer from vertical diffusion limitations known to occur in high aspect ratio rectilinear wells [39] limiting their use for cell culture. The ability to successfully proliferate cells in microbubbles with aspect ratio ~3 suggests sufficient nutrient and waste exchange occurs through the microbubble opening.

3.4 Effects of conditioned media on HaCaT morphology

To provide further evidence that cells in microbubbles secrete soluble factors that can influence their function, we investigated the effect of seeding HaCaT cells in microbubbles and on planar PDMS using conditioned media. Conditioned DMEM was harvested as described in Section 2.6, and serially diluted with normal DMEM (0–100%). As mentioned above, HaCaT cells cultured on planar PDMS form compact spheroids but they do not transition to a sheeting morphology. However, when HaCaT cells are cultured on planar PDMS with increasing amounts of conditioned DMEM a sheeting morphology results (Fig. 5). Bright-field images (Figs. 5A, B and C) and corresponding fluorescence images (Figs. 5D, E and F) are shown for HaCaT cells cultured in 100% DMEM (Fig. 5I), 50% DMEM – 50% conditioned DMEM (Fig. 5II) and 100% conditioned DMEM (Fig. 5III). Other ratios of conditioned media are shown in Supplementary Fig. 6S. We observed that both the size and the number of spheroids decreases with increasing conditioned media concentration (Supplementary Fig. 7S). Live/dead staining also indicated a spheroid size threshold of >50–100 microns diameter for the presence of a necrotic center (Supplementary Fig. 6S). Striking differences in colony morphology can also be seen for cells seeded in microbubbles and cultured in 100% conditioned media (Fig. 6). At the end of 24 hours cells cultured in 100% DMEM (Fig. 6 **panel I**) formed spheroids on both planar PDMS (Fig. 6A) and in microbubbles (Fig. 6E) as opposed to 100% conditioned DMEM (Fig. 6 **panel II**) where sheeting is immediately adopted on both planar PDMS and in microbubbles (Figs. 6B, F). These findings further support soluble factors present in conditioned DMEM impact colony morphology.

3.5 Effects of TGF-β and calcium on HaCaT morphology

To investigate the identity of soluble factors that may influence HaCaT colony morphology we considered both TGF-β1 and calcium. TGF-β1 is a protein known to regulate cell proliferation, growth, differentiation and motility as well as to promote cells to synthesis and deposit extracellular matrix which are important factors in the EMT process [29, 40]. Calcium is a key driver of keratinocyte differentiation and is required for E-cadherin function [41]. We observed that when cells were cultured in DMEM with 10 ng/mL of TGF-β1 (Fig. 6 **panel III**) a sheeting morphology was immediately adopted on planar PDMS (Fig. 6C) and in microbubbles (Fig. 6G). Interestingly, when HaCaT cells were cultured in calcium-free DMEM (Fig. 6 **panel IV**), they were unable to form a single tightly packed spheroid; instead they largely remained as a greater number of small spheroids on planar

PDMS (Fig. 6D) and as individual cells in microbubbles (Fig. 6H) These results suggest that calcium is required for compact spheroid formation presumably through the formation of cell-cell junctions and that the change in spheroid to sheeting morphology can be brought about by secretion TGF-β1 which is consistent with previous studies [31, 32, 42, 43].

3.6 Dependence of E-cadherin expression on HaCaT morphology transition

To support the above findings we investigated the expression of E-cadherin which is a calcium dependent key regulator of cell-cell junction in keratinocytes. The inability of HaCaT cells to form spheroids on planar PDMS and microbubbles in the absence of calcium suggests a loss of cell-cell adhesion [44]. Loss of cell-cell contacts and E-cadherin expression are important hallmarks associated with EMT in cancer metastasis regulated by the tumor microenvironment [45]. Figure 7 shows representative bright- field and fluorescence images for E-cadherin staining of HaCaT cells in a single microbubble as a function of time. Cells were observed to be in a compact spheroid by the end of 24 hours (Fig. 7A) and in a sheeting morphology by the end of 96 hours (Fig. 7B). The corresponding fluorescence images of HaCaT cells stained with FITC conjugated anti-cadherin-E antibody show a strong E-cadherin cortical staining for HaCaT spheroids (Fig. 7C) as opposed to a weak and diffuse staining for E-cadherin exhibited by HaCaT cells in sheeting morphology (Fig. 7D). These data suggest that the morphology transition of HaCaT cells in microbubbles is EMT-like and accompanied by a decrease of E-cadherin expression.

4. Discussion

To advance studies in tissue formation, function, and disease development, novel in vitro 3D cell culture systems are needed that can enable identification of important molecular signatures and elucidate the interplay of soluble factors in the microenvironment. Among the several types of cell culture systems that have been designed to mimic the in vivo microenvironment, the most popular methods involve the use of microfluidics-based 3D cell culture micro-bioreactors [20, 46–48]. The merits of 3D cell culture systems over conventional 2D cell culture have been established [49–51]. However, microfluidics based 3D cell culture technology is still in the early stages of development and unlikely to bring about a paradigm shift replacing conventional 2D cell culture techniques [52]. A key consideration in the design of in vitro cell culture systems is the media volume to cell ratio which is an important factor that drives cell survival, proliferation and function. Cells rely on secretion of soluble factors (i.e. growth factors, cytokines) to encourage adhesion and proliferation, particularly in foreign environments where cells must synthesize their own matrix. In vitro when cells are seeded onto unfavorable (hydrophobic) substrates they may migrate to form cell-cell contacts for survival. A parallel in cancer metastasis is the self reliance of the tumor initiating cell(s) to interact and condition the microenvironment for survival and subsequent proliferation. The dormancy associated with tumor micrometastases suggests a delay in this process [53].

In this work we exploited silicon wafer fabrication technology and gas expansion molding recently introduced [24, 25], to demonstrate PDMS microbubbles as a novel 3D cell culture platform. Previously we showed melanoma cells proliferate throughout the microbubble to form homogenously sized microtumors [25]. The ability of seeded cells to proliferate in microbubbles with high aspect ratio ~3 suggests sufficient nutrient and waste exchange occurs through the microbubble opening. In this study, we demonstrate the unique property of the microbubble architecture that allows HaCaT cells to condition their microenvironment through secretion and accumulation of soluble factors. We observed a lower limit on the number of cells (~10 cells) that must be seeded into a hydrophobic microbubble (~8 nL and 100 μm diameter circular opening) for cell survival and spheroid formation which equates to a media volume to cell ratio of ~1 nL/cell. Future studies will test using additional cell types

and microbubble sizes the effect of microbubble volume and opening size to determine the generality of this ratio. When 10–25 HaCaT cells are seeded and cultured in microbubbles they initially form spheroids with increased expression of E-cadherin, forming extensive cell-cell junctions required for survival. This response initiates because PDMS is a hydrophobic substrate that does not favor HaCaT cell adhesion and spreading. By the end of 72 hours HaCaT cells undergo a fascinating morphology change (Fig.1 D–F and Fig 2) in which they sheet along the interior microbubble surface. The change in morphology is similar to the EMT phenomenon that occurs in cancer cell metastasis and is considered to be highly regulated by the tumor microenvironment [30]. HaCaT cells are an immortalized human keratinocyte cell line that is extensively used in cancer research and is considered to be a very good model cell line for studying epithelial cancers [54, 55]. We attribute this EMT-like transition to the accumulation of soluble factors, including TGF-β, enabled by the unique microbubble architecture. Presence of Ca^{2+} is also required for spheroid formation. A typical microbubble used in these experiments had a diameter of 250 μm and a volume of ~8 nL. Seeding 20 cells in this microbubble is equivalent to a seeding density of ~1×10^4 cells/cm^2 considering the entire microbubble surface area. This equates to ~0.4 nL of media / cell. For comparison, seeding cells at a similar density in a 96-well plate (~3259 cells/well) yields a value of about ~31 nL of media / cell (100 μL and 0.32 cm^2 per well). The ~75X smaller volume of media per cell ratio in the microbubble combined with the persistence of a shallow concentration gradient (Fig. 4) allows for soluble factors secreted by cells to accumulate to bioactive levels despite media exchange with the bulk reservoir that occurs through the microbubble opening. We attribute the failure of HaCaT spheroids formed on planar PDMS to undergo the sheet morphology transition to the inability of cells to condition their media in the 96 well TCP. We also observed in microbubbles that the time required for the morphology transition to occur decreased with increasing cell seeding density. This is consistent with the notion that the concentration of soluble factors rises to bioactive levels more rapidly (Fig. 3).

To further investigate factors that may contribute to morphology transition we performed experiments with conditioned DMEM and DMEM spiked with TGF-β1. The role of TGF-β has been thoroughly characterized in tumors [29,40] and it has been shown to affect keratinocyte differentiation and proliferation state when cultured in high calcium media [31]. Three TGF-β isoforms are differentially expressed in HaCaT keratinocytes and their role has been elucidated in skin carcinogenesis [56]. TGF-β1 causes an epithelial to mesenchymal transition in HaCaT characterized by the loss of epithelial junction proteins and an increase in their migratory potential [32, 43]. Recently, it was shown that TGF-β1 induces EMT in HaCaT keratinocytes downregulating epithelial markers such as E-cadherin and ZO-1 [32]. When, HaCaT cells were cultured on planar PDMS in conditioned DMEM they immediately sheeted and formed spreading cell clusters (Fig. 5). Similarly, HaCaT cells seeded in microbubbles also adopted a sheeting morphology from the onset when cultured in conditioned media or media spiked with TGF-β1 (Figs. 6F, G). The ability of HaCaT cells to start sheeting without exhibiting interim spheroid morphology in conditioned media suggests the presence of soluble factors with TGF-β1 being an important contributor. Calcium concentration is also an important contributor of colony morphology. When HaCaT cells were cultured in no calcium DMEM on planar PDMS and in microbubbles cells appeared as small clusters or individual cells respectively and failed to adopt a sheeting morphology (Figs. 6D, H). The inability of cells to assume the spheroidal morphology is consistent with their inability to form cell-cell adhesions via calcium dependent E-cadherin binding. We studied the expression of E-cadherin in HaCaT cells cultured in microbubbles as a function of time (Fig. 7) and found a correlation between the spheroid to sheeting morphology transition and a decrease of E-cadherin staining, as expected from literature [32, 42, 43]. The phenomenon observed parallels the epithelial to mesenchymal transition that

occurs in tumor metastasis suggesting microbubble technology as a convenient means to further investigate such processes in a controlled microenvironment.

5. Conclusions

Developing a novel cost-effective 3D cell culture platform which enables control over the physical aspects of the microenvironment and allows cells to rapidly condition their microenvironment by secreting soluble factors has great potential in understanding normal and diseased tissue function. In this study microbubbles were shown as a 3D compartment ideally suited to study how cells interact with and condition their microenvironment through autocrine signaling. Immortalized human keratinocyte cell line (HaCaT) cultured in microbubbles exhibited a spheroid to sheeting morphology transition within 72 hrs. Cells cultured on planar PDMS in 96 well plate also form spheroids but they do not undergo a morphology transition even after 6 days in culture. This was shown experimentally and theoretically to result from secreted factor accumulation in the microbubble that rises to bioactive levels. It was observed that kinetics of the morphology transition depended on the number of cells seeded per microbubble. Results found TGF-β1 and Ca^{2+} to be important factors that drive this morphology change. The spheroid to sheeting transition observed resembles the epithelial-to-mesenchymal transition that occurs in tumors with down regulation of E-cadherin expression. Although microbubble technology is still in the early stages of development, the results presented suggest the possibility of this 3D cell culture technique to possibly bring about a paradigm shift in the current methodology used to investigate cell microenvironmental effects important in normal and diseased tissues.

Supplementary Material

Refer to Web version on PubMed Central for supplementary material.

Acknowledgments

The authors would like to thank Dr. Karl Kasischke and Gheorghe Salahura (University of Rochester Medical Center, Rochester, NY) for their expertise in multiphoton microscopy. The authors would also like to thank funding support from the NSF CBET 0827862.

References

1. Abbott DE, Bailey CM, Postovit L-M, Seftor EA, Margaryan N, Seftor REB, et al. The epigenetic influence of tumor and embryonic microenvironments: How different are they? Cancer Microenviron. 2008; 1:13–21. [PubMed: 19308681]
2. Walker GM, Zeringue HC, Beebe DJ. Microenvironment design considerations for cellular scale studies. Lab Chip. 2004; 4:91–97. [PubMed: 15052346]
3. Hung PJ, Lee PJ, Sabounchi P, Aghdam N, Lin R, Lee LP. A novel high aspect ratio microfluidic design to provide a stable and uniform microenvironment for cell growth in a high throughput mammalian cell culture array. Lab Chip. 2005; 5:44–48. [PubMed: 15616739]
4. Polyak K, Kalluri R. The role of the microenvironment in mammary gland development and cancer. Cold Spring Harb Perspect Biol. 2010; 2(11):a003244. [PubMed: 20591988]
5. Discher DE, Mooney DJ, Zandstra PW. Growth factors, matrices, and forces combine and control stem cells. Science. 2009; 324(5935):1673–1677. [PubMed: 19556500]
6. Laconi E. The evolving concept of tumor microenvironments. Bioessays. 2007; 29(8):738–744. [PubMed: 17621638]
7. Zent, R.; Pozzi, A. New York, NY: Springer Science+Business Media, LLC; 2010. SpringerLink (Online service). Cell-extracellular matrix interactions in cancer. Available from: http://dx.doi.org/10.1007/978-1-4419-0814-8

8. Schedin P, Elias A. Multistep tumorigenesis and the microenvironment. Breast Cancer Res. 2004; 6(2):93–101. [PubMed: 14979914]
9. Whiteside TL. The tumor microenvironment and its role in promoting tumor growth. Oncogene. 2008; 27(45):5904–5912. [PubMed: 18836471]
10. Brabek J, Mierke CT, Rosel D, Vesely P, Fabry B. The role of the tissue microenvironment in the regulation of cancer cell motility and invasion. Cell Commun Signal. 2010; 8:22. [PubMed: 20822526]
11. Farrow B, Albo D, Berger DH. The role of the tumor microenvironment in the progression of pancreatic cancer. J Surg Res. 2008; 149(2):319–328. [PubMed: 18639248]
12. Ghotra VP, Puigvert JC, Danen EH. The cancer stem cell microenvironment and anti-cancer therapy. Int J Radiat Biol. 2009; 85(11):955–962. [PubMed: 19895272]
13. Brown JM. Tumor microenvironment and the response to anticancer therapy. Cancer Biol Ther. 2002; 1(5):453–458. [PubMed: 12496469]
14. Sun T, Jackson S, Haycock JW, MacNeil S. Culture of skin cells in 3D rather than 2D improves their ability to survive exposure to cytotoxic agents. J Biotechnol. 2006; 122(3):372–381. [PubMed: 16446003]
15. Park TH, Shuler ML. Integration of cell culture and microfabrication technology. Biotechnol Prog. 2003; 19(2):243–253. [PubMed: 12675556]
16. Andersson H, van den Berg A. Microfabrication and microfluidics for tissue engineering: state of the art and future opportunities. Lab Chip. 2004; 4(2):98–103. [PubMed: 15052347]
17. Lee J, Cuddihy MJ, Kotov NA. Three-dimensional cell culture matrices: State of the art. Tissue Eng Part B Rev. 2008; 14(1):61–86. [PubMed: 18454635]
18. Jang JH, Schaffer DV. Microarraying the cellular microenvironment. Mol Syst Biol. 2006; 2:39. [PubMed: 16820780]
19. Flaim CJ, Chien S, Bhatia SN. An extracellular matrix microarray for probing cellular differentiation. Nat Methods. 2005; 2(2):119–125. [PubMed: 15782209]
20. Figallo E, Cannizzaro C, Gerecht S, Burdick JA, Langer R, Elvassore N, et al. Micro-bioreactor array for controlling cellular microenvironments. Lab Chip. 2007; 7(6):710–719. [PubMed: 17538712]
21. Lee JH, Chung S, Kim SJ, Han J. Poly(dimethylsiloxane)-based protein preconcentration using a nanogap generated by junction gap breakdown. Anal Chem. 2007; 79(17):6868–6873. [PubMed: 17628080]
22. Yu CB, Pan XP, Li LJ. Progress in bioreactors of bioartificial livers. Hepatobiliary Pancreat Dis Int. 2009; 8(2):134–140. [PubMed: 19357025]
23. Tanaka Y, Morishima K, Shimizu T, Kikuchi A, Yamato M, Okano T, et al. Demonstration of a PDMS-based bio-microactuator using cultured cardiomyocytes to drive polymer micropillars. Lab Chip. 2006; 6(2):230–235. [PubMed: 16450032]
24. Giang UBT, Lee D, King MR, DeLouise LA. Microfabrication of cavities in polydimethylsiloxane using DRIE silicon molds. Lab Chip. 2007; 7(12):1660–1662. [PubMed: 18030383]
25. Giang UBT, King MR, DeLouise LA. Microfabrication of Bubbular Cavities in PDMS for Cell Sorting and Microcell Culture Applications. J Bionic Eng. 2008; 5(4):308–316.
26. Lin RZ, Chang HY. Recent advances in three-dimensional multicellular spheroid culture for biomedical research. Biotechnol J. 2008; 3(9–10):1172–1184. [PubMed: 18566957]
27. Yamada KM, Cukierman E. Modeling tissue morphogenesis and cancer in 3D. Cell. 2007; 130:601–610. [PubMed: 17719539]
28. Kalluri R, Weinberg RA. The basics of epithelial-mesenchymal transition. J Clin Invest. 2009; 119(6):1420–1428. [PubMed: 19487818]
29. Massague J. TGFbeta in Cancer. Cell. 2008; 134(2):215–230. [PubMed: 18662538]
30. Tse JC, Kalluri R. Mechanisms of metastasis: epithelial-to-mesenchymal transition and contribution of tumor microenvironment. J Cell Biochem. 2007; 101(4):816–829. [PubMed: 17243120]

31. Cho HR, Hong SB, Kim YI, Lee JW, Kim NI. Differential expression of TGF-beta isoforms during differentiation of HaCaT human keratinocyte cells: implication for the separate role in epidermal differentiation. J Korean Med Sci. 2004; 19(6):853–858. [PubMed: 15608397]
32. Rasanen K, Vaheri A. TGF-beta1 causes epithelial-mesenchymal transition in HaCaT derivatives, but induces expression of COX-2 and migration only in benign, not in malignant keratinocytes. J Dermatol Sci. 2010; 58(2):97–104. [PubMed: 20399617]
33. Thorne RG, Hrabetova S, Nicholson C. Diffusion of epidermal growth factor in rat brain extracellular space measured by integrative optical imaging. J Neurophysiol. 2004; 92(6):3471–3481. [PubMed: 15269225]
34. Jeong HW, Kim IS. TGF-beta1 enhances betaig-h3-mediated keratinocyte cell migration through the alpha3beta1 integrin and PI3K. J Cell Biochem. 2004; 92(4):770–780. [PubMed: 15211574]
35. Clapham DE. Calcium signaling. Cell. 2007; 131(6):1047–1058. [PubMed: 18083096]
36. Hirano S, Nose A, Hatta K, Kawakami A, Takeichi M. Calcium-dependent cell-cell adhesion molecules (cadherins) - subclass specificities and possible involvement of cctin bundles. J Cell Biol. 1987; 105(6):2501–2510. [PubMed: 3320048]
37. Lee JN, Park C, Whitesides GM. Solvent compatibility of poly(dimethylsiloxane)-based microfluidic devices. Anal Chem. 2003; 75(23):6544–6554. [PubMed: 14640726]
38. Sutherland RM. Cell and environment interactions in tumor microregions - the multicell spheroid model. Science. 1988; 240(4849):177–184. [PubMed: 2451290]
39. Moeller HC, Mian MK, Shrivastava S, Chung BG, Khademhosseini A. A microwell array system for stem cell culture. Biomaterials. 2008; 29(6):752–763. [PubMed: 18001830]
40. Xu J, Lamouille S, Derynck R. TGF-beta-induced epithelial to mesenchymal transition. Cell Res. 2009; 19(2):156–172. [PubMed: 19153598]
41. Lewis JE, Jensen PJ, Wheelock MJ. Cadherin function is required for human keratinocytes to assemble desmosomes and stratify in response to calcium. J Invest Dermatol. 1994; 102(6):870–877. [PubMed: 8006450]
42. Herfs M, Hubert P, Kholod N, Caberg JH, Gilles C, Berx G, et al. Transforming growth factor-β1-mediated slug and snail transcription factor up-regulation reduces the density of langerhans cells in epithelial metaplasia by affecting E-cadherin expression. Am J Pathol. 2008; 172(5):1391–1402. [PubMed: 18385519]
43. Davies M, Robinson M, Smith E, Huntley S, Prime S, Paterson I. Induction of epithelial to mesenchymal transition in human immortal and maligant keratinocytes by TGF-β1 involves MAPK, Smad and AP-1 signalling pathyways. J Cell Biochem. 2005; 95:918–931. [PubMed: 15861394]
44. Amagai M. Adhesion Molecules .1. Keratinocyte-geratinocyte interactions - cadherins and pemphigus. J Invest Dermatol. 1995; 104(1):146–152. [PubMed: 7798634]
45. Cicchini C, Laudadio I, Citarella F, Corazzari M, Steindler C, Conigliaro A, et al. TGFbeta-induced EMT requires focal adhesion kinase (FAK) signaling. Exp Cell Res. 2008; 314(1):143–152. [PubMed: 17949712]
46. Hung PJ, Lee PJ, Sabounchi P, Aghdam N, Lin R, Lee LP. A novel high aspect ratio microfluidic design to provide a stable and uniform microenvironment for cell growth in a high throughput mammalian cell culture array. Lab Chip. 2005; 5(1):44–48. [PubMed: 15616739]
47. Wong AP, Perez-Castillejos R, Christopher Love J, Whitesides GM. Partitioning microfluidic channels with hydrogel to construct tunable 3-D cellular microenvironments. Biomaterials. 2008; 29(12):1853–1861. [PubMed: 18243301]
48. Lin Z, Cherng-Wen T, Roy P, Trau D. In-situ measurement of cellular microenvironments in a microfluidic device. Lab Chip. 2009; 9(2):257–262. [PubMed: 19107282]
49. Derda R, Laromaine A, Mammoto A, Tang SK, Mammoto T, Ingber DE, et al. Paper-supported 3D cell culture for tissue-based bioassays. Proc Natl Acad Sci U S A. 2009; 106(44):18457–18462. [PubMed: 19846768]
50. Margulis A, Zhang W, Alt-Holland A, Pawagi S, Prabhu P, Cao J, et al. Loss of intercellular adhesion activates a transition from low- to high-grade human squamous cell carcinoma. Int J Cancer. 2006; 118(4):821–831. [PubMed: 16152579]

51. Pedersen JA, Swartz MA. Mechanobiology in the third dimension. Ann Biomed Eng. 2005; 33(11):1469–1490. [PubMed: 16341917]

52. Wu MH, Huang SB, Lee GB. Microfluidic cell culture systems for drug research. Lab Chip. 2010; 10(8):939–956. [PubMed: 20358102]

53. Aguirre-Ghiso JA. Models, mechanisms and clinical evidence for cancer dormancy. Nat Rev Cancer. 2007; 7(11):834–846. [PubMed: 17957189]

54. Ren Q, Kari C, Quadros MR, Burd R, McCue P, Dicker AP, et al. Malignant transformation of immortalized HaCaT keratinocytes through deregulated nuclear factor kappaB signaling. Cancer Res. 2006; 66(10):5209–5215. [PubMed: 16707445]

55. Castro NE, Lange CA. Breast tumor kinase and extracellular signal-regulated kinase 5 mediate Met receptor signaling to cell migration in breast cancer cells. Breast Cancer Res. 2010; 12(4):R60. [PubMed: 20687930]

56. Gold LI, Jussila T, Fusenig NE, Stenback F. TGF-beta isoforms are differentially expressed in increasing malignant grades of HaCaT keratinocytes, suggesting separate roles in skin carcinogenesis. J Pathol. 2000; 190(5):579–588. [PubMed: 10727984]

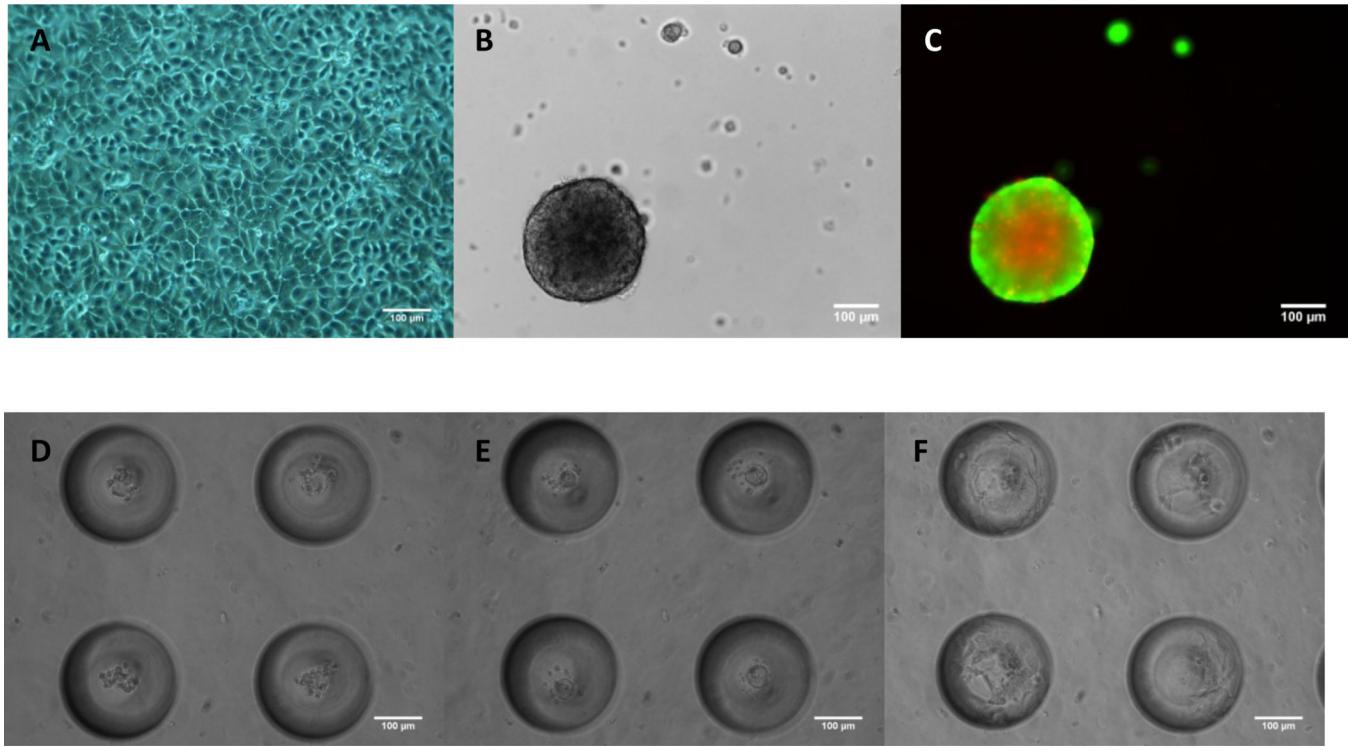

Fig.1.

HaCaT cells propagated as a 2D monolayer on TCP (A). 3D spheroids on planar PDMS (B). Fluorescent field image indicated a dead cell core (Red – Propidium Iodide) and a live cell periphery (Green – Calcein AM) (C). Morphology of HaCaT cells cultured in MB at the end of 4h (D), 24h (E) and 72h (F) showed that cells cultured in MB underwent a change in morphology with time. Seeding density = 2×10^4 cells/cm^2. Scale bars = 100 µm.

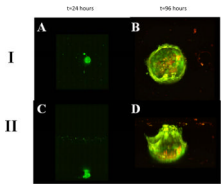

Fig. 2.

Top view (I) and Side view (II) images from a multiphoton microscope of a single microbubble seeded with HaCaT cells at 2×10^4 cells/cm^2 at the end of 24h [(A) and (C)] 96h [(B) and (D)]. Cells were stained with Calcein-AM (live, green) and Propidium Iodide (dead, red).

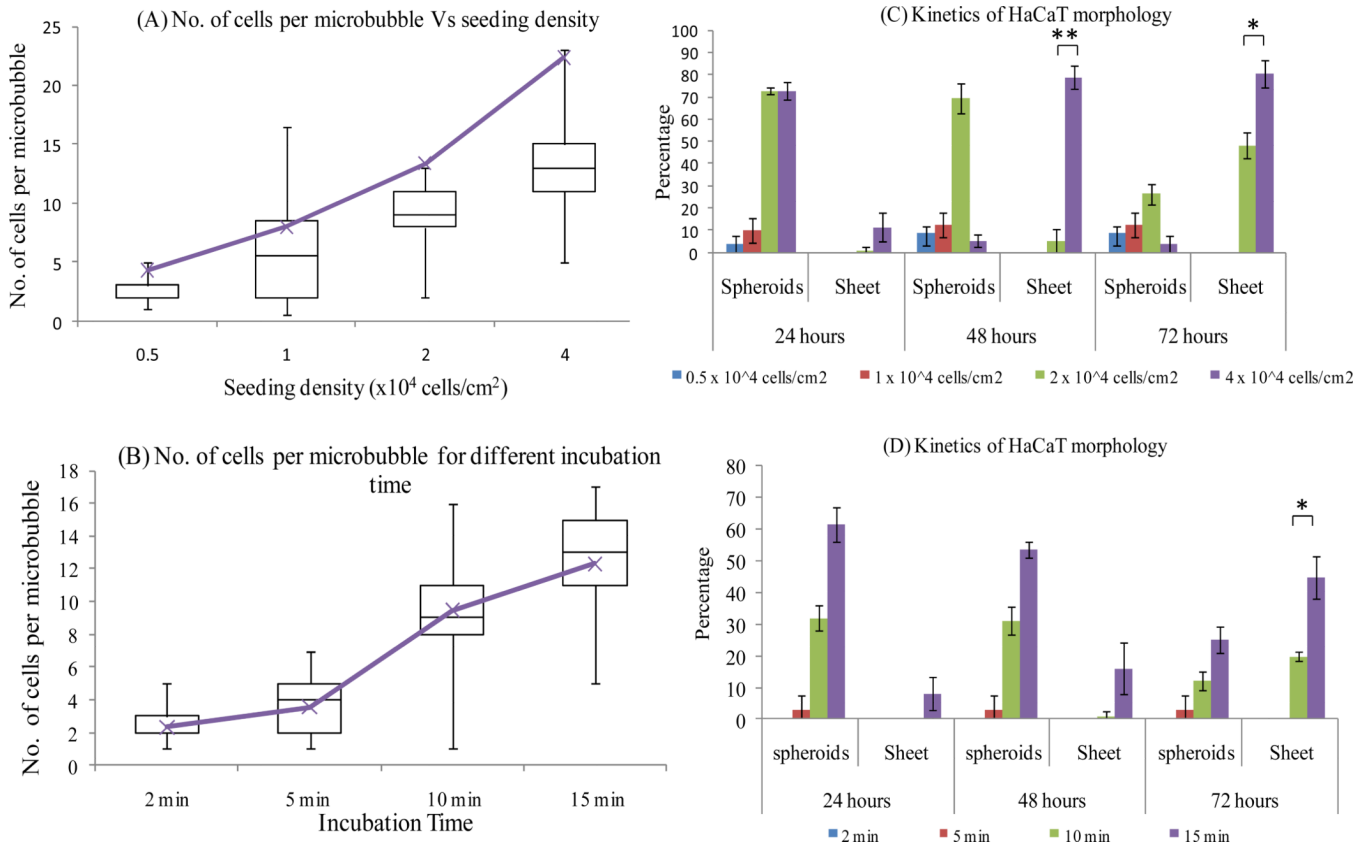

Fig. 3.

The morphology of HaCaT cells is largely determined by the number of cells per microbubble (MB). Box and whisker plot showing number of cells per MB for varying seeding density for a fixed incubation time of 15 min (A) [Purple line indicates average number of cells per MB]. Bar graph showing the percentage of MB showing spheroid or sheeting morphology at different time points for varying seeding density (B) n=114 MB. Box and whisker plot indicating the distribution of number of cells per MB for varying incubation time at a fixed seeding density of 2×10^4 cells/cm^2 (C) [Purple line indicates average number of cells per MB]. Bar graph showing the percentage of MB showing spheroid or sheet morphology at different time points for varying incubation time (D) n=114 MB (* $p<0.05$, ** $p<0.01$).

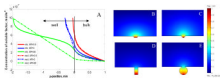

Fig. 4.
COMSOL simulation results contrasting the vertical concentration profile through microbubble and rectilinear wells as a function of well depth (y-position = 0 corresponds to the well opening) for three aspect ratios (A). Graphical representation of the concentration of soluble factors at steady state for rectilinear and microbubble wells with aspect ratios 0.5 (B and C, respectively) and aspect ratio 3.0 (D and E, respectively).

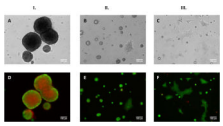

Fig. 5.

Bright-field [(A), (B) and (C)] and corresponding fluorescence [(D), (E) and (F)] [Calcein-AM (green/live) Propidium Iodide (red/dead)] images of HaCaT cells cultured on planar PDMS. Images were taken at the end of 24h on cells cultured in 100% DMEM (I.) 50% DMEM-50% Conditioned DMEM (II.) and 100% Conditioned DMEM (III.) [Scale Bar = 100 μm; seeding density = 2×10^4 cells/cm^2].

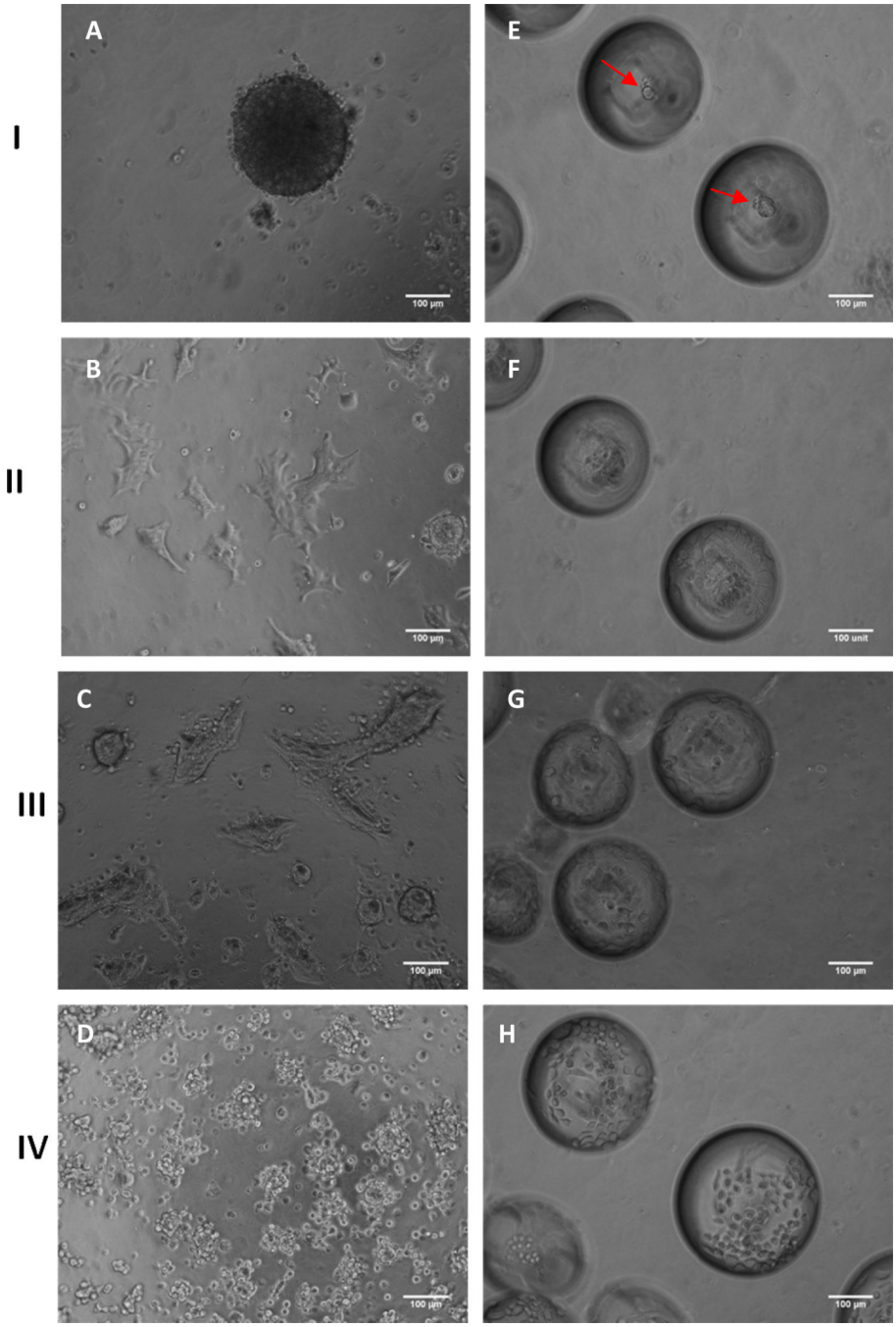

Fig. 6.

Morphology of HaCaT cells on planar PDMS (A–D) and microbubbles (MB) (E–H) at the end of 24h cultured in DMEM (I), 100% conditioned DMEM (II), DMEM with 10ng/mL TGF-β1 (III), and no calcium DMEM (IV). HaCaT cells formed a compact tight spheroid on planar PDMS and MB (red arrows pointing to spheroids) when cultured in DMEM [(A) and (E)]. HaCaT cells tended to propagate as spreading cell clusters on planar PDMS when cultured in 100% conditioned DMEM (B) and DMEM with 10ng/mL TGF-β1 (C). In contrast to (A) cells assumed a sheeting morphology on MB when cultured in 100% conditioned DMEM (F) and DMEM with 10ng/mL TGF-β1 (G). In no calcium DMEM cells

largely remained small spheroids on planar PDMS (D) and individual cells on MB (H). [Scale Bars = 100 μm; seeding density =2×10^4 cells / cm^2].

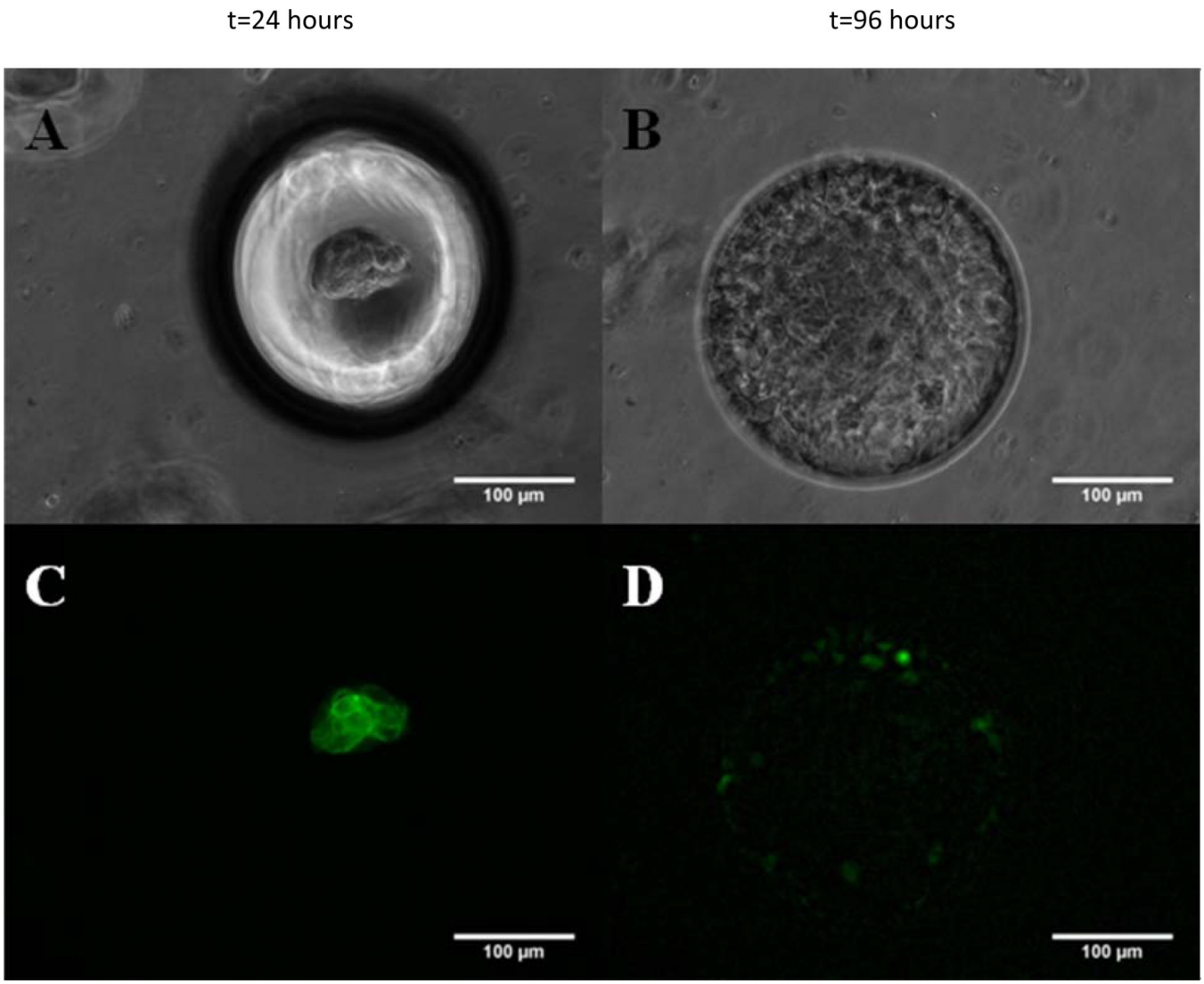

Fig. 7.

Spheroid to sheeting transition is characterized by the loss of E-Cadherin expression. Bright-field images of a single microbubble focused on the bottom of microbubbles (A) focused on the opening of microbubbles (B) and corresponding fluorescence [(C) and (D)] images of MB seeded with HaCaT cells. Cells were stained with FITC conjugated anti-Cadherin-E antibody. HaCaT spheroids (24h) show a strong cortical staining for E-Cadherin; mean fluorescent intensity per unit area (MFI) 19.43 ± 3.79, n=3 images (C) and HaCaT sheets (96h) show a relatively weak and diffuse staining pattern for E-Cadherin; MFI= 5.15 ± 3.78, n=3 images (D). [Seeding density =2×10^4 cells/cm^2; Scale Bar = 100 μm].